[Frontiers in Bioscience 14, 2193-2202, January 1, 2009]

Combined microPET/CT for imaging of hepatocellular carcinoma in mice

Christian von Falck[1,2], Thomas Rodt[1,2], Roman Halter[2], Reinhard Spanel[3], Michael Galanski[1], Juergen Borlak[2]

[1]Institute of Radiology, Hannover Medical School, Hannover, Germany, [2]Department of Pharmaceutical Research and Medical Biotechnology, Fraunhofer Institute for Toxicology and Experimental Medicine, Hannover, Germany, [3]Institute of Pathology, Viersen, Germany

TABLE OF CONTENTS

1. ABSTRACT

The EGF-transgenic mouse is a genetic model of hepatocellular carcinoma that allows for a comprehensive study of signal pathways, molecular interactions and the evaluation of novel therapeutic concepts. In this regard, non-invasive imaging tools for serial *in-vivo* monitoring of tumor load and growth are highly desirable. This study therefore aimed at demonstrating the feasibility of non-invasive *in-vivo* imaging of primary liver malignancies in mice using combined contrast-enhanced microCT and F-18 FDG microPET. In our murine disease model, microCT enabled imaging of primary liver tumors down to a lesional diameter of 0.9mm. F-18 FDG tumor-to-non-tumor ratio of HCCs was observed to be dependent on lesion size and linked to overpression of glucose transporters and hexokinase isoenzymes as determined by gene expression studies. Histopathologic analyses indicated an increased cellular dedifferentiation with increase lesion size, as well.

2. INTRODUCTION

Hepatocellular carcinoma (HCC) is the most frequent primary malignancy of the liver. It usually develops following a cascade of chronic liver injury including inflammation, regeneration, remodeling, fibrosis and, ultimately, irreversible cirrhosis. The most prominent risk factors are chronic hepatitis B and C infection (80%), Aflatoxin B1 exposure, alcohol-induced cirrhosis, hemochromatosis, fatty liver disease and alpha-1 antitrypsin deficiency. Therapeutic concepts with curative intention are mainly surgical and often limited to early stages of disease. Liver transplantation is a curative option for a subset of patients with locally advanced disease that meet the milan criteria. Different treatments applying systemic, local or combined delivery of chemotherapeutics and local ablative procedures have been described for later stages of disease, but their mid- to long-term results remain unsatisfying (1,2).

The ability to develop effective treatments requires the availability of relevant preclinical models to evaluate novel agents and approaches with respect to their activity against tumor. Different animal models have been established and allow for a comprehensive study of signal pathways, molecular interactions and the evaluation of novel therapeutic concepts. The EGF-transgenic mouse is a genetic model, that develops multiple highly malignant HCCs through targeted overexpression of a secretable form of epidermal growth factor (IgEGF) in hepatocytes (3). It mimics effectively the consequence of altered EGF signaling via the EGF receptor. There is strong evidence, that overexpression of liver mitogens like EGF or TGF-alpha may be an important mechanism in the development of HCC (4, 5). Recently, an oncogenomic study with EGF transgenic mice was reported. Essentially, genome-wide gene expression analysis at different stages of the disease enabled an improved understanding of the molecular events associated with EGF-induced HCC and an identification of novel therapeutic targets (6). In this regard, *non-invasive* preclinical imaging techniques are highly desirable as tools to monitor tumor growth and response to therapeutic interventions. As the use of contrast-enhanced microCT and ^{18}F-FDG microPET has not yet been described for imaging of primary liver cancer in rodents, the rationale of this study was: 1. To demonstrate the feasibility of imaging *primary* liver malignancies *in-vivo* using contrast-enhanced micro computed tomography (microCT) and (^{18}F)-2-fluoro-2-deoxyglucose (F-18 FDG) micro positron emission tomography (microPET) in a genetic mouse model of hepatocellular carcinoma and 2. to assess correspondence of ^{18}F-FDG uptake with expression of glucose transporters and hexokinase isoenzymes.

3. MATERIALS AND METHODS

3.1. Tumor model and animal handling

All animal studies were approved by the institutional ethics committee and the local governmental authorities and were in accordance with national guidelines. The EGF- transgenic mouse model has been previously described in detail (3,6). Mice were maintained as hemizygotes in the Blk6 background. Transgenicity was confirmed by PCR of DNA extracted from tail biopsies. Mice were kept in cages with 1 – 4 mice per cage on sawdust on a 12-h light-dark cycle, at 50% relative humidity, in a temperature controlled (22°C) room. The animals received irradiated rodent chow and drinking water ad libitum. All imaging procedures were performed under inhalation anaesthesia with isoflurane (Isoba vet., Essex Pharma, Germany) at a concentration of 5% for anesthesia induction and 1-2% for maintenance. Animals breathed spontaneously via nose cone (Summit Anesthesia Solutions, Bend, OR, USA). The breathing rate was continuously monitored using a small pressure transducer (Biovet, m2m imaging, Newark, NJ, USA) and the mice were placed on a temperature controlled pad for warming (T/Pump, Gaymar, Orchard Park, NY, USA). Recovery time after the imaging procedure was usually less than five minutes.

3.2. *In vivo* Imaging

MicroCT and ^{18}F-FDG microPET examinations were performed in 12 mice (age: 7.5±0.7 months, sex: m=5 / f=7). Follow-up examinations after two-weeks were performed in a subgroup of 5 mice (age: 7.5±0.5 months) to evaluate our imaging approach with regard to monitoring tumor growth.

3.3. microCT imaging

Mice were injected through the tail vein with approximately 200 - 300µl (10µl/g bodyweight) of a liver-specific iodinated contrast agent (DHOG, Fenestra LC, ART Inc., Saint-Laurent, Canada) 4 hours prior to the imaging procedure. The timing of injection and image acquisition was selected on the basis of manufacturer's guidelines, previously published studies (7) and personal experience (unpublished data). The microCT scan was obtained with a high-resolution small animal computed tomography scanner (eXplore Locus, GE Healthcare, Chalfont St. Giles, UK) immediately after the microPET scan. Misregistration artefacts were mimimized by using a multi-modality cradle that can be easily interchanged between the different scanners. Scan parameters were: tube voltage: 80kVp, tube current: 450µA, projections: 720, exposure time: 400ms, one average per frame. No respiratory gating was used. Total scan duration was 18 minutes for a single gantry rotation, covering an axial field-of-view of 33 mm. Image data was reconstructed using a cone-beam algorithm on an 8-node linux cluster. The resulting voxel size of the isotropic dataset was 45µm. Arbitrary attenuation values were converted to the Hounsfield scale using a calibration phantom with water, air and bone inserts.

3.4. microPET imaging

All animals were fasted for at least 6h prior to the imaging procedure. Anaesthesized mice received an injection of 10MBq (^{18}F)-2-fluoro-2-deoxyglucose (^{18}F-FDG, Department of Nuclear Medicine, Hannover Medical School, Hannover, Germany) in a total volume of 50 – 100µl sterile isotonic saline solution into the tail vein. Static images were acquired after 60 minutes using a high-resolution small animal PET camera (eXplore Vista, GE Healthcare, Chalfont St. Giles, UK). Total acquisition time was 30 minutes for a single bed position. Images were corrected for random events and scatter prior to reconstruction with a 3D-FORE/2D-OSEM iterative algorithm. No attenuation correction and no respiratory gating were used.

3.5. Image analysis and Statistics

MicroCT datasets were visualized and evaluated using the software Microview 1.2 (GE Healthcare, Chalfont St. Giles, UK). Rigid registration of PET and CT datasets based on anatomical landmarks (First galley + Professional galley + Licensed PDF was used to generate fused datasets. Image evaluation included assessment of contrast enhancement and detection and measurement of focal liver lesions. Lesion quantification was based on 2D-measurements of the largest diameter. Measurements were performed by two readers and the results were averaged. MicroPET datasets were evaluated using the software MMWKS (GE Healthcare, Chalfont St. Giles, UK). Following registration and image fusion,

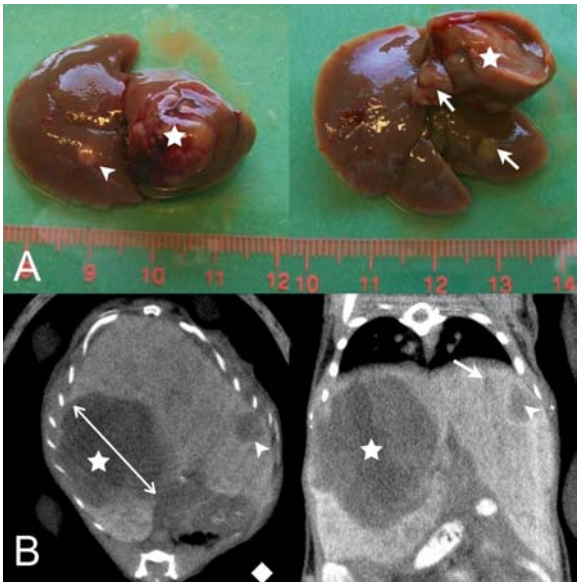

Figure 1. Typical appearance of multifocal hepatocellular carcinomas in the genetic murine disease model. Macroscopically (A) multiple, exophytic lesions can be seen on the surface of the explanted liver (arrows). The corresponding microCT of the same animal (B) was obtained after the injection of a liver-specific contrast agent, which leads to opacification of regular liver parenchyma. HCC lesions are depicted as hypodense areas, that often show an irregular pattern with a peripheral rim (arrows).

regions-of-interest (ROI) were manually defined in all focal liver lesions as detected by microCT and/or ^{18}F-FDG microPET. In large, partially cystic lesions, the ROI was placed in the solid part of the tumor. The background (non-tumor) signal was determined by placing large ROI in the tumor-free liver parenchyma. The maximum count rate per volume was determined for each ROI and tumor-to-non-tumor ratios were calculated. Small lesions (<=5mm) were corrected for partial volume effects according to their size on microCT using precalculated recovery coefficients and technical specifications of the microPET scanner (8,9). Liver lesions were separated into three groups according to their size: small (<5mm), medium (5-10mm) and large (>10mm) lesions. The mean tumor-to-non-tumor ratio and the standard deviation were calculated. The students unpaired two-sided t-test was used to evaluate the statistical significance (p-value cutoff determined as 0.05).

3.6. Necropsy and histopathology

Mice were euthanized after the imaging procedure and the liver was removed for gross examination and histological analysis. Tumor tissue was fixed in 4% formaldehyde in PBS and embedded in paraffin. Paraffin blocks were sectioned into 3-5µm thick slices and stained with haematoxylin alone (H), haematoxylin and eosin (HE) and Ladewig's procedure. Single slices were additionally stained with periodic acid Schiff stain (PAS), Elastic van Giessen stain (EvG) and reticulin stain.

3.7. Gene Expression Analysis

Global gene expression was analyzed in a different group of EGF transgenic (n=6) and wild-type (n=4) mice using the Affymetrix Gene Chip technology. In brief, total RNA was isolated from frozen tumor tissue. Double-stranded cDNA was synthesized and used to generated biotin-labelled cRNA. The cRNA was fragmented and hybridized onto the Murine Genome U74Av2 array. After standard washing and staining procedures the arrays were analyzed using the Agilent GeneArray scanner. The Affymetrix Micoarrays Suite 5.0 was used for data analysis. Expression levels of glucose transporters (*glut-1*, *glut-3*) and hexokinase isoenzymes (*hexokinase I / II*) in small (<5mm; n = 5; pooled), medium (5 - 10mm; n = 4) and large (>10mm; n = 3) liver tumors were compared to transgenic, but non-tumorous liver tissue and wild-type animals. A total of 12 analyses for large tumors (3 tumors vs. 4 controls), 16 analyses for medium sized tumors (4 tumors vs. 4 controls), 4 analyses for small tumors (5 pooled tumors vs. 4 controls) and 12 analyses for tumor-free transgenic tissue (3 livers vs. 4 controls) were performed. Fold-change (FC) values were calculated as the ratio of the average expression levels for each gene between two tissue sets.

4. Results

4.1. In-vivo imaging: microCT

A total of 57 liver lesions were detected in 12 examinations with contrast-enhanced microCT with an average of 4.7 tumors (± 2.3; range: 2 - 8) per animal and a lesion size varying between 0.9mm and 23mm (long axis diameter). Mean lesion size was 2.3mm (± 1.1mm) for small (<5mm; n = 34), 6.9mm (± 1.6mm) for medium (5 - 10mm; n = 9) and 14.5mm (± 4.1mm; n = 14) for large tumors. The morphologic appearance of the tumors was primarily hypodense. Small lesions were mostly homogenous, whereas larger lesions demonstrated areas of intermediate contrast uptake, that could be differentiated from tumor-free liver parenchyma. These areas were usually located either at the tumor periphery or as linear structures in the central parts of the lesion (Figure 1, 2). Large tumors with hypodense areas in CT showed typically pseudocystic intratumorous peliosis and necrosis in histopathology (Figure 2).

4.2. *In vivo* imaging: microPET

To allow for a more accurate anatomical localization of focal ^{18}F-FDG uptake, we performed registration and fusion of microCT and microPET datasets prior to quantitative analysis of PET data. The additional information from contrast-enhanced microCT enabled differentiation of physiological tracer uptake from true pathologic findings as illustrated in Figure 2. The exact anatomical correlation was especially helpful at the esophageal-gastric junction due to its close anatomical relationship to the liver and the high physiological uptake. Fused datasets demonstrated that ^{18}F-FDG uptake was absent in large parts of the tumor with hypodense appearance in contrast-enhanced microCT. However, ^{18}F-FDG uptake was intense in peripheral parts of the tumors with intermediate uptake of the contrast agent in microCT. In ^{18}F-FDG microPET the average tumor-to-non-tumor

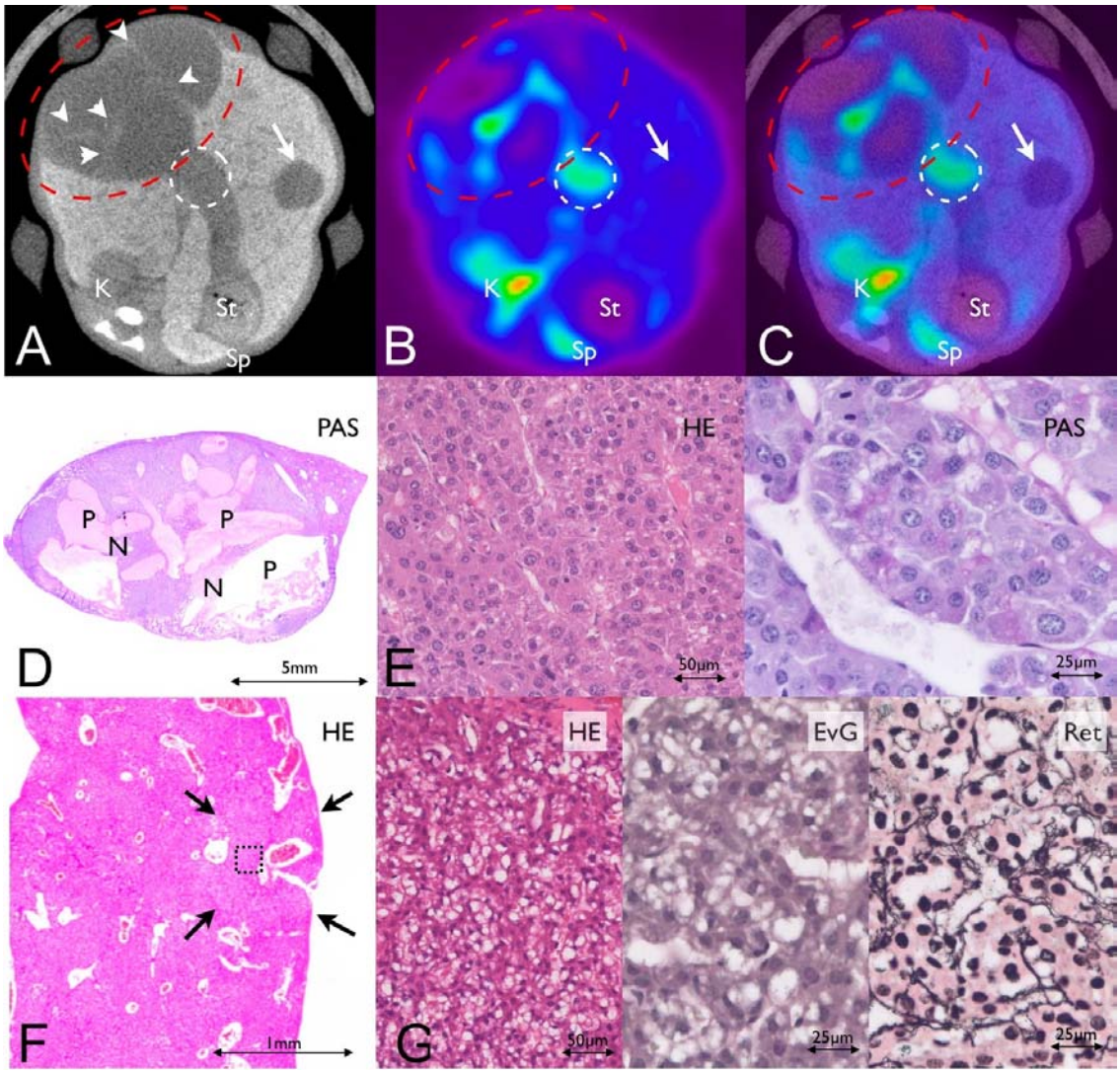

Figure 2. Typical appearance of multifocal HCCs in the combined imaging approach. The liver lesions are sharply depicted in the contrast-enhanced microCT (A). Note the irregular contrast enhancement of the large lesion (red circle) with slightly hyperdense, web-like structures within a large hypodense area. The small lesion (arrow) is uniform hypodense. The corresponding ^{18}F-FDG microPET image (B) shows an intense increase in glucose metabolism in the large liver lesion (red circle), whereas the small lesion (0.9mm, arrow) shows no significant tracer uptake. The PET/CT fusion image (C) clearly illustrates, that the uptake of ^{18}F-FDG in the liver is focused on slightly hyperdense structures within the large lesion. Notably, only the fused image allows to differentiate physiological uptake at the esophago-gastric junction (white circle) and the kidneys from pathologic tracer accumulation. D, E: Typical histological appearance of the large subcapsular HCC with cystic alterations due to multifocal pseudocystic intratumorous peliosis (P) and necrosis (N) in the scanned slide (D). Higher magnification (E) shows solid and trabecular growth pattern with multilayered trabeculae and severe polymorphism. F, G: Typical histological appearance of the small subcapsular lesion (F), classified as an early HCC. Higher magnification (G) shows destruction of normal liver architecture and substitution with irregular, mainly bilayered trabeculae. Only slight nuclear atypia. Pronounced vacuolar lipidisation. Reticuline fibres (Ret) mark the distorted sinus of the tumor. *K=kidney, St=stomach, Sp=spleen, P=peliosis, N=necrosis, PAS=periodic acid Schiff stain, HE=haematoxylin & eosin stain, EvG=Elastic van Giessen stain, Ret=reticulin stain (Gomori).*

ratio was 1.05 (± 0.27) for small, 1.21 (± 0.33) for medium and 1.87 (± 0.53) for large tumors (s. Figure 4b), respectively. Differences were statistically significant for large lesions as compared to small and medium sized lesions ($p < 0.01$). There was no statistically significant difference between medium and small lesions.

4.3. Imaging of tumor growth

Follow-up examinations were performed in a subgroup of 5 transgenic mice with microCT-proven liver lesions after an interval of 14 days. A total of 16 lesions (medium: $n = 3$; small: $n = 13$) could be identified. Rapid tumor growth was seen with all lesions with a mean

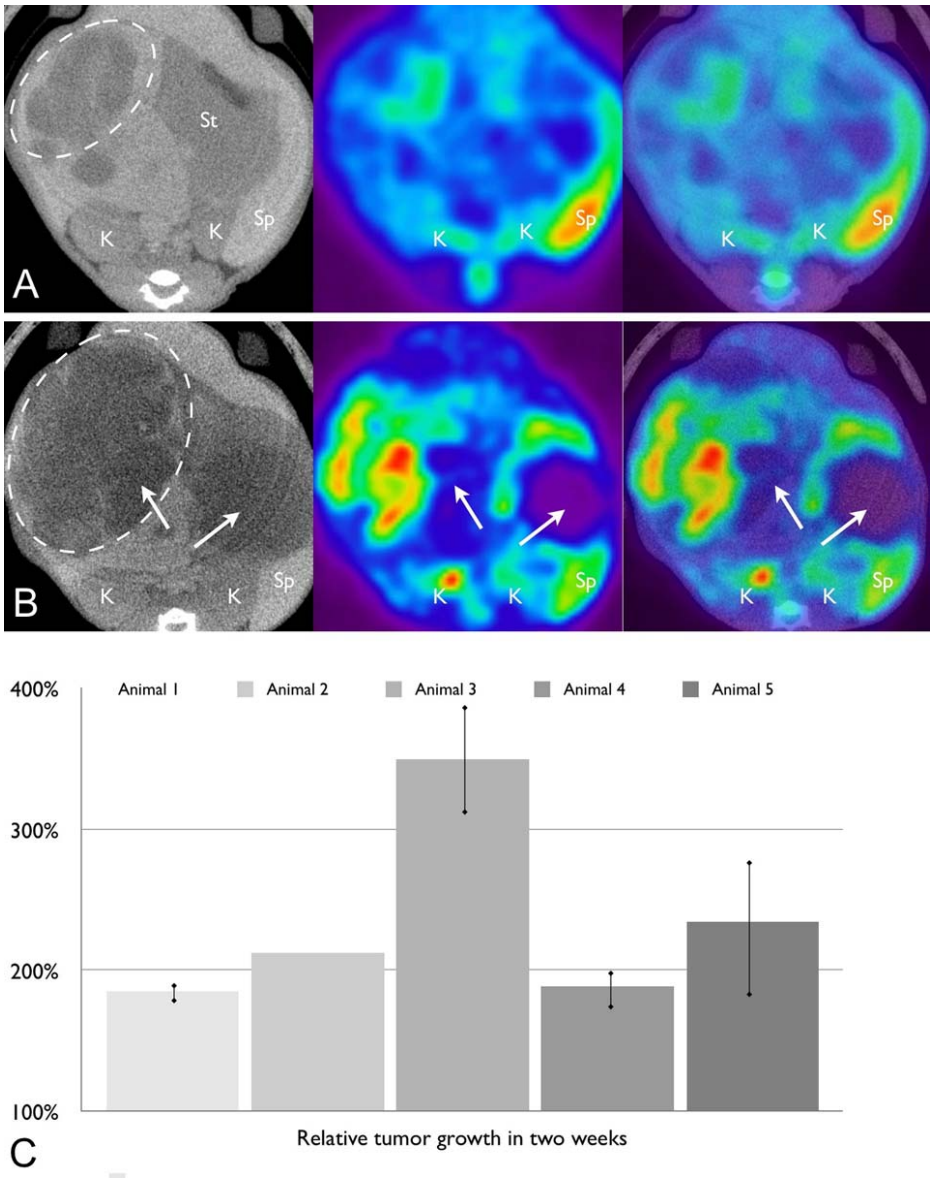

Figure 3. A. Contrast-enhanced microCT (left), ^{18}F-FDG microPET (middle) and fused image of a baseline (A) and follow-up examination after two weeks (B) in an EGF-transgenic mouse. Note the rapid increase in tumor size (microCT) as well as in glucose utilization (^{18}F-FDG microPET, circle). Again, the uptake of ^{18}F-FDG is mainly focused on the parts of the lesions that have a more solid appearance in microCT with an intermediate contrast enhancement, whereas the cystic/necrotic parts of the tumor do not show any accumulation of ^{18}F-FDG (arrows). C.Growth kinetics of all 5 mice over a period of two weeks. Except for animal 2 (only one tumor present), the growth of all tumors per animal is averaged. Error bars indicate standard deviation.

increase in the axial diameter of 86.6% (± 75,1%; $p<0.05$) (s. Figure 3a, b). Corresponding microPET demonstrated a mean increase in tumor-to-non-tumor ratio of 23.9% (± 29.4%; $p<0.05$). Heterogeneity in growth kinetics was observed and contributed to the relatively high standard deviation. Individual growth kinetics of the 5 mice are depicted in figure 3c. Except for one animal with a single tumor, tumor growth is given as mean growth of all tumors per animal.

4.4. Expression of glucose transporters and hexokinases

Expression of the glucose transporters *glut-1* and *glut-3* as well as the glycolytic enzymes *hexokinase-1* and *hexokinase-2* was analyzed separately for small, medium and large tumors and tumor-free transgenic livers and compared to normal liver tissue of wild-type mice (s. Fig 4a). In small and medium tumors, *hexokinase-1* was moderately overexpressed (fold change (FC) = 2.4 (small) / 2.3 (medium), $p<0.05$) as compared with wild-type mice. No relevant change was noted for *glut-1*, *glut-3* or *hexokinase-2* (FC < 2). In large tumors, however, expression of *hexokinase-1* increased further (FC = 3.7; $p<0.05$). Additionally, expression of *glut-1* and *hexokinase-2* were strongly increased (glut-1: FC = 5.7; hexokinase-2:

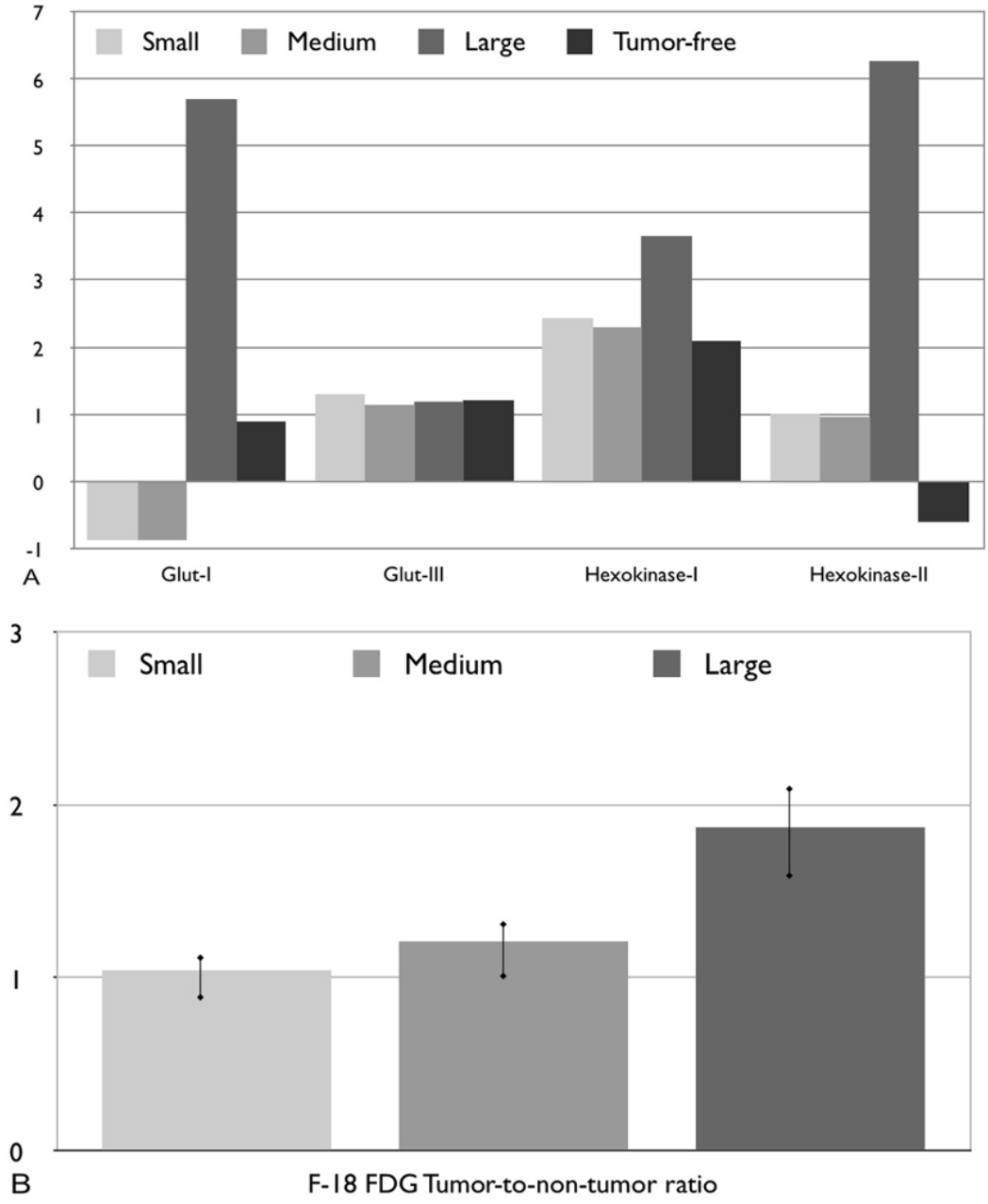

Figure 4. A. Expression of glucose carriers *glut-I* and *glut-III* as well as *hexokinase* isoenzymes I / II in the genetic disease model of hepatocellular carcinoma compared to wild-type mice. Expression levels are given as fold change (FC) and separated according to tumor size. Note the significant overexpression of *glut-I*, *hexokinase-I* and *hexokinase-II* in large tumors compared to medium and small tumors. The elevated expression level of *hexokinase-I* in small and medium sized lesions are assumed to results from the increased proliferative background activity in the liver of our genetic tumor model, as a comparable increase is seen in tumor-free transgenic parenchyma, as well. B.Tumor-to-non-tumor ratios of hepatocellular carcinoms in ^{18}F-FDG microPET according to lesion size (small <5mm; medium 5 – 10mm; large > 10mm). Large lesions show a significantly increased tumor-to-non-tumor ratio of ^{18}F-FDG compared to medium and small tumors (p<0.05).

FC = 6.3), aswell. No significant change was observed for tumor-free transgenic parenchyma when compared with wild-type animals. This data fits well with the results from the microPET studies, where a significant increase in 18F-FDG uptake was noted for large lesions, only.

4.5. Histopathology

Macroscopically, all examined mice developed multiple tumors of different size, which could be microscopically identified as HCC. Tumors ranged from highly to less differentiated. In general, small HCCs were

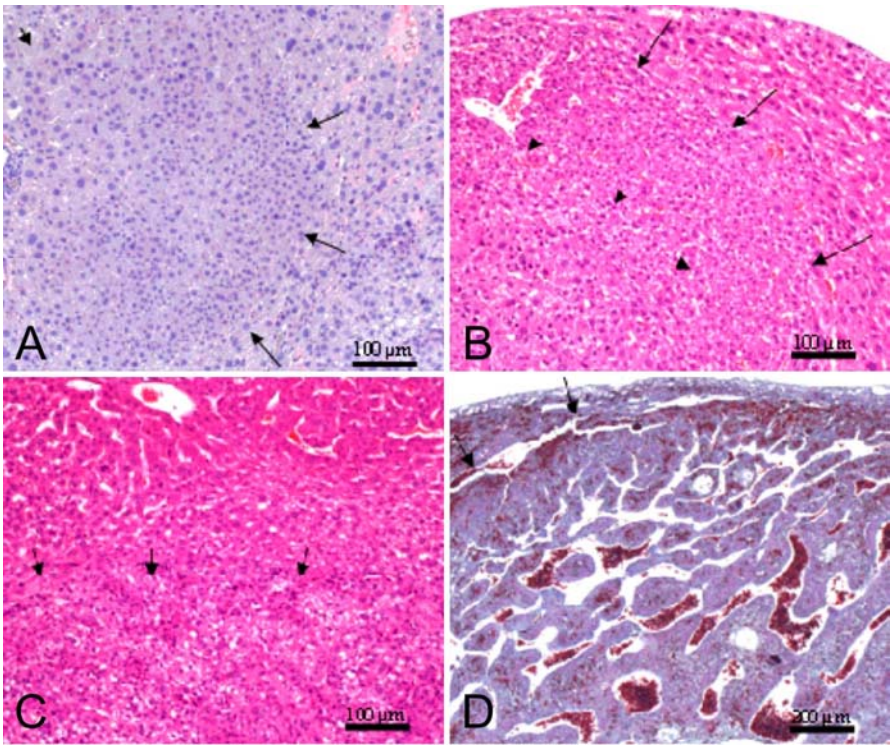

Figure 5. Histology of tumors and precursor lesions of the liver in EGF-transgenic mice: Nomenclature according to literature[19]. (A) Basically diffuse Large Cell Dysplasia in tumor-free parenchyma of transgenic mice: Enlarged hepatocytes with enlarged nuclei. One of multiple nodular precancerous lesions, a so called Dysplastic Nodule: Small proliferations with slight to moderate nuclear atypia (low grade intraepithelial neoplasia (long arrows), focally with transition intro larger cells with severe nuclear atypia (high grade intraepithelial neoplasia (short arrows). (B) Remnant of a dysplastic nodule (arrows) at the edge of an early HCC with marked nuclear atypia and at least bilayered trabeculae (arrowheads). (C) Small well differentiated adenoma-like HCC: Slight to moderate polymorphism and lipid vacuolisation; irregular, mainly bilayered trabeculae and consuming growth at the edge (arrows) . (D) Advanced large HCC with multilayered trabeculae and increased polymorphism: Complete destruction of the original liver architecture and radial growth at the edge (arrows) .*Magnifications see bar*. *Staining H (A), H&E (B, C), Ladewig (D)*

adenoma-like tumors with well-developed hepatocytes and mainly bilayered trabeculae, whereas larger HCCs showed advanced cellular dedifferentiation, enhanced nuclear atypia and multilayered trabeculae (Figure 2, 5). Cystic degeneration which represented in fact an intratumorous pseudocystic peliosis and confluent necrosis were seen in larger tumors, only. The precursor lesions followed a regular developmental pattern in the transgenic EGF2-model: Basically, the tumor-free liver parenchyma presented large cell dysplasia with large hepatocytes and enlarged, repeatedly polymorphous nuclei. Its ubiquitous, rather diffuse appearance in the transgenic animals contrasted with the multiple consecutive nodular cell proliferations, so called dysplastic foci and nodules (according to human classification) (10).

5. DISCUSSION

Genetic disease models are invaluable for preclinical testing of novel anticancer drugs. In the past, mostly small animal models were established in immunodeficient nude mice by subcutaneous injection of tumor cells (e.g. xenotransplants). However, these models suffer from severe restrictions in terms of data translation to clinical research and the rather unphysiological tumor environment. More relevant models involve either implanting (orthotopic) tumors cells into an organ of interest or, particularly, the use of genetic animal models, where disease candidate genes and processes associated with malignant transformation can be investigated (11,12). However, the difficulty in using many of these animal models in the preclinical testing of novel anticancer drugs is the limited ability to accurately monitor development and growth of intraabdominal or visceral tumors without having to sacrifice the study animal. Here, we characterized a genetic mouse model of hepatocellular carcinoma by means of non-invasive *in-vivo* imaging techniques. Through combined contrast-enhanced microCT and ^{18}F-FDG microPET we were able to visualize tumor load and growth of the primary liver malignancies. Furthermore, we were able to demonstrate correspondence of glucose transporter and hexokinase expression with tumor-size dependent uptake of ^{18}F-FDG and histopathological findings. This mouse model together with the imaging platform may serve as a scenario for the evaluation of novel therapeutic approaches.

Micro computed tomography (microCT) is a morphologic imaging modality that depicts the anatomical features of different pathologies in great detail (13). Through serial examinations and volumetric measurements, microCT can serve as a powerful method to detect and monitor tumor burden and assess the therapeutic efficacy in small animal disease models (13-15). As in clinical CT imaging, contrast agents are mandatory for imaging of parenchymal organs due to the poor low-contrast performance of non-enhanced CT. Due to the long scan time of most commercially available microCT equipment and the rapid renal clearance of water-soluble iodinated contrast agents, liver-specific, long-lasting contrast agents are often required (7, 16, 17). Preclinical imaging of liver lesions in murine disease models with contrast-enhanced microCT has been described for metastatic disease of pheochromocytoma (18) and colon cancer (7). In both studies, microCT imaging was performed after the injection of an iodinated hepatobiliary contrast agent (1,3-bis (7- (3-amino-2,4,6-triiodophenyl) heptanoyl)-2-oleoyl-glycerol, ITG) as initially described by Weber *et al.* (19). Through an ApoE receptor-mediated pathway this contrast-agent is selectively taken up into hepatocytes and leads to opacification of normal liver parenchyma. Hepatic metastases are thus depicted as hypodense areas as the metastatic cells do not express the ApoE receptor (7). However, unlike for orthotopic tumor implants, the use of ITG to image *primary* liver malignancies has not been reported, yet. Depending on the degree of differentiation, these primary tumors have the potential to accomplish hepatocyte-specific functions. It is known from gadolinium-based liver-specific contrast media for magnetic resonance imaging that highly differentiated HCCs tend to show an uptake of liver-specific contrast agents (20, 21). This observation for liver specific contrast agents may help to explain the microCT appearance of the liver lesions in our genetic murine disease model. Through correlation of microCT with ^{18}F-FDG microPET we were able to demonstrate that the solid parts of large tumors show an intermediate contrast-enhancement and can be differentiated from hypodense areas that correspond to necrotic or cystic parts of the tumor as well as from regular liver parenchyma with hyperdense appearance. Histopathology demonstrated necrotic or pseudocystic peliosis in these hypodense areas (Fig.2). Furthermore, we were able to demonstrate that serial contrast enhanced microCT examinations can be used to visualize changes in tumor size in our disease model through morphometric measurements. Side-by-side reading allows for comparison of microCT datasets acquired at different time points and enables lesion-by-lesion follow-up for RECIST- or WHO-like evaluation of therapeutic efficacy. Semi-automatic 3D volumetry tools are available and may allow a more precise measurement of tumor load and growth. However, in this work we relied on 2D measurements to allow comparability with our previous work (6)

(^{18}F)-2-fluoro-2-deoxyglucose positron emission tomography (^{18}F-FDG PET) is a metabolic imaging method that depicts the glucose metabolism of tissues and organs. It is well known, that most malignant tumors show an increased uptake of ^{18}F-FDG due to enhanced glucose utilization (22). In general, ^{18}F-FDG uptake in malignant tissue largely depends on the presence of glucose transporters and the glycolytic enzyme hexokinase (22). It is known, that HCCs show a heterogeneous biological and clinical behavior that is reflected in the variable uptake patterns of HCC in ^{18}F-FDG PET. Increased uptake of ^{18}F-FDG is only seen in about half of hepatocellular carcinoma patients (23-25). However, it has been demonstrated that ^{18}F-FDG uptake is closely linked to the pathologic grading in HCC and that clinical outcome is poorer in HCC patients with a high tumor-to-non-tumor ^{18}F-FDG ratio (26). In patients with cirrhosis and HCC scheduled for liver transplantation, ^{18}F-FDG PET is helpful for estimating the post-transplantation risk of tumor recurrence, reflecting its ability to differentiate between different grades of biological aggressiveness (27). Comparable to these results from clinical PET, ^{18}F-FDG uptake in HCC lesions in our murine disease model was not uniform, but dependent on lesion size and the degree of differentiation (26). We found for small liver lesions a glucose metabolism comparable to regular liver parenchyma. A significant increase in ^{18}F-FDG uptake is seen particularly in large tumors (>10mm). These results were in concordance with gene expression data, where a significant overexpression of *glut-1*, *hexokinase-1* and *hexokinase-2* was observed in large tumors, only. As previously described, it is well known from clinical studies, that the uptake of ^{18}F-FDG in HCC is closely linked to the degree of differentiation (25, 26). Our histopathologic evaluation demonstrates increasing cellular dedifferentiation of the hepatocellular carcinomas with expanding lesion size (Fig 2, 6), as recently reported (6). As our tumor model follows a well-defined genetic program based on EGF mitotic signalling, the link between lesion size and degree of dedifferentiation can be regarded as rather uniform.Indeed, contrast-enhanced microCT allowed for visualization and monitoring of tumor growth in our transgenic disease model; the practical application of serial microCT studies, especially in combination with microPET may, however, be limited due to the biological effects of the ionizing radiation (28, 29). The influence of cumulative radiation exposure through repeated studies on tumor development and therapeutic response has not been evaluated for our combined imaging approach, as yet. Further studies are therefore on the way to evaluate the usability of our imaging approach in preclinical therapy studies. In conclusion, combined contrast-enhanced microCT and ^{18}F-FDG microPET imaging allows the *in-vivo* visualization of tumor burden and growth in a genetic mouse model of hepatocellular carcinoma. ^{18}F-FDG tumor-to-non-tumor ratio is dependent on tumor size and in concordance with expression levels of glucose transporters and hexokinases.

6. ACKNOWLEDGMENTS

We gratefully acknowledge the support by GE Healthcare.

7. REFERENCES

1. Schafer DF, Sorrell MF: Hepatocellular carcinoma.

Lancet 353, 1253-1257 (1999)

2. Avila MA, Bersain C, Sangro B, Priteo J: New therapies for hepatocellular carcinoma. *Oncogene* 25, 3866-3884 (2006)

3. Tonjes RR, Lohler J, O'Sullivan JF, Kay GF, Schmidt GH, Dalemans W, Pavirani A, Paul D. Autocrine mitogen IgEGF cooperates with c-myc or with the Hcs locus during hepatocarcinogenesis in transgenic mice. *Oncogene* 104, 765–768 (1995)

4. Wang Y, Ripperger J, Fey GH, Samols D, Kordula T, Wetzler M, Van Etten RA, Baumann H. Modulation of hepatic acute phase gene expression by epidermal growth factor and Src protein tyrosine kinases in murine and human hepatic cells. *Hepatology* 30, 682-692 (1999)

5. Ostrowski J, Woszczynski M, Kowalczyk P, Wocial T, Henning E, Trzeciak L, Janik P, Bomsztyk K. Increased activity of MAP, p70S6 and p90rs kinases is associated with AP-1 activation in spontaneous liver tumours, but not in adjacent tissue in mice. *Br J Cancer* 82, 1041–1050 (2000)

6. Borlak J, Meier T, Halter R, Spanel R, Spanel-Borowski K. Epidermal growth factor-induced hepatocellular carcinoma: gene expression profiles in precursor lesions, early stage and solitary tumours. *Oncogene* 24, 1809–1819 (2005)

7. Weber SM, Peterson KA, Durkee B, Qi C, Longino M, Warner T, Lee FT Jr, Weichert JP. Imaging of murine liver tumor using microCT with a hepatocyte-selective contrast agent: accuracy in dependent on adequate contrast enhancement. *J Surg Res* 119, 41-45 (2004)

8. Kessler RM, Ellis JR, Eden M. Analysis of Emission Tomographic Scan Data: Limitations Imposed by Resolution and Background. J Comput Assist Tomogr 8, 514-522 (1984)

9. Wang Y, Seidel J, Tsui BM, Vaquerro JJ, Pomper MG. Performance evaluation of the GE Healthcare eXplore VISTA dual-ring small-animal PET scanner. J Nucl Med 47, 1891-1900 (2006)

10. (no authors listed). Terminology of nodular hepatocellular lesions. International Working Party. *Hepatology 22, 983-993 (1995)*

11. Becher OJ, Holland EC. Genetically engineered models have advantages over xenografts for preclinical studies. *Cancer Res 66, 3355-3358 (*2006)

12. Sharpless NE, Depinho RA. The mighty mouse: genetically engineered mouse models in cancer drug development. *Nat Rev Drug Discov* 5, 741-754 (2006)

13. Paulus MJ, Gleason SS, Kennel SJ, Hunsicker PR, Johnson DK. High resolution X-ray computed tomography: an emerging tool for small animal cancer research. *Neoplasia* 2, 62-70 (2000)

14. Chang CH, Jan ML, Fan KH, Wang HE, Tsai TH, Chen CF, Fu YK, Lee TW. Longitudinal evaluation of tumor metastasis by an FDG-microPET/microCT dual-imaging modality in a lung carcinoma-bearing mouse model. *Anticancer Res.* 26, 159-166 (2006)

15. Cody DD, Nelson CL, Bradley WM, Wislez M, Juroske D, Price RE, Zhou X, Bekele BN, Kurie JM. Murine lung tumor measurement using respiratory-gated micro-computed tomography. *Invest Radiol.* 40, 263-269 (2005)

16. Ford NL, Graham KC, Groom AC, Macdonald IC, Chambers AF, Holdsworth DW. Time-Course Characterization of the Computed Tomography Contrast Enhancement of an Iodinated Blood-Pool Contrast Agent in Mice Using a Volumetric Flat-Panel Equipped Computed Tomography Scanner. *Invest Radiol.* 41, 384-390 (2006)

17. Montet X, Pastor CM, Vallée JP, Becker CD, Geissbuhler A, Morel DR, Meda P. Improved visualization of vessels and hepatic tumors by micro-computed tomography (CT) using iodinated liposomes. *Invest Radiol* 42, 2236-2241 (2007)

18. Ohta S, Lai EW, Morris JC, Bakan DA, Klaunberg B, Cleary S, Powers JF, Tischler AS, Abu-Asab M, Schimel D, Pacak K. MicroCT for high-resolution imaging of ectopic pheochromocytoma tumors in the liver of nude mice. *Int J Cancer 119, 2236-2241 (*2006)

19. Weichert JP, Longino MA, Bakan DA, Spigarelli MG, Schwendner SW, Francis IR, Counsell RE. Targeted polyiodinated triglycerides for hepatic computed tomography. Invest Radiol 29, Suppl 2: S284-285 (1994)

20. Huppertz A, Haraida S, Kraus A, Zech CJ, Scheidler J, Breuer J, Helmberger TK, Reiser MF. Enhancement of focal liver lesions at gadoxetic acid-enhanced MR imaging: correlation with histopathologic findings and spiral CT – initial observations. *Radiology* 234, 468-478 (2005)

21. Saito K, Kotake F, Ito N, Ozuki T, Mikami R, Abe K, Shimazaki Y. Gd-EOB-DTPA enhanced MRI for hepatocellular carcinoma: quantitative evaluation of tumor enhancement in hepatobiliary phase. *Magn Reson Med Sci* 4, 1-9 (2005)

22. Pauwels EK, Sturm EJ, Bombardieri E, Cleton FJ, Stokkel MP. Positron-emission tomography with (18F)fluordeoxyglucose. Part I. Biochemical uptake mechanism and its implication for clinical studies. *J Cancer Res Clin Oncol* 126, 549-559 (2000)

23. Trojan J, Schroeder O, Raedle J, Baum RP, Herrmann G, Jacobi V, Zeuzem S. Fluorine-18 FDG positron emission tomography for imaging of hepatocellular carcinoma. *Am J Gastroenterol* 94, 3314-3319 (1999)

24. Jeng LB, Changlai SP, Shen YY, Lin CC, Tsai CH, Kao CH. Limited value of 18F-2-deoxyglucose positron

emission tomography to detect hepatocellular carcinoma in hepatitis B virus carriers. *Hepato-Gastroenterology* 50, 2154-2156 *(*2003)

25. Torizuka T, Tamaki N, Inokuma T, Magata Y, Sasayama S, Yonekura Y, Tanaka A, Yamaoka Y, Yamamoto K, Konishi J. *In vivo* assessment of glucose metabolism in hepatocellular carcinoma with FDG-PET. *J Nucl Med* 36, 1811-1817 (1995)

26. Lee JD, Yun M, Lee JM, Choi Y, Choi YH, Kim JS, Kim SJ, Kim KS, Yang WI, Park YN, Han KH, Lee WJ, Yoo N, Lim SM, Park JH. Analysis of gene expression profiles of hepatocellular carcinomas with regard to F-18-FDG uptake pattern on positron emission tomography. *Eur J Nucl Med Mol Imaging* 31, 1621-1630 (2004)

27. Yang SH, Suh KS, Lee HW. The role of (18F)-FDG-PET imaging for the selection of liver transplantation candidates among hepatocellular carcinoma patients. *Liver Transpl* 12, 1655-1660 (2006)

28. Taschera u R, Chow PL, Chatziioannou AE. Monte carlo simulations of dose from microCT imaging procedures in a realistic mouse phantom. *Med Phys* 33, 216-224 (2006)

29. Funk T, Sun M, Hasegawa BH. Radiation dose estimate in small animal SPECT and PET. *Med Phys* 31, 2680-2686 (2004)

Key Words microPET, microCT, Hepatocellular Carcinoma, Mouse

Send correspondence to: Christian von Falck, Department of Radiology, Hannover Medical School, Carl-Neuberg-Strasse 1, 30625 Hannover, Germany, Tel: 49-511-532-3687, Fax: 49-511-532-3797, E-mail: c.v.falck@gmx.de